Diagn Interv Radiol 2026; DOI: 10.4274/dir.2026.264036

BREAST IMAGING

ORIGINAL ARTICLE

Comparing clinicopathological factors and quantitative background parenchymal enhancement to predict pathological complete response after neoadjuvant chemotherapy in breast cancer

Süleyman Öncü[1]
Murat Yüce[2]
Ahmet İrfan Temur[1]

[1]University of Health Sciences Türkiye, Bakırköy Dr. Sadi Konuk Training and Research Hospital, İstanbul, Türkiye

[2]Biomedical Engineering and Imaging Institute, Icahn School of Medicine at Mount Sinai, New York, United States of America

Corresponding author: Süleyman Öncü

E-mail: suleymanoncu32@gmail.com

Received 02 April 2026; revision requested 28 April 2026; last revision requested 29 June 2026; accepted 27 July 2026.

Epub: 14.09.2026

DOI: 10.4274/dir.2026.264036

PURPOSE

To investigate the predictive value of deep learning (nnU-Net)-based fully automated quantitative background parenchymal enhancement (BPE) metrics and clinicopathological factors for pathological complete response (pCR) in patients with breast cancer receiving neoadjuvant chemotherapy (NACT).

METHODS

This retrospective study included 142 patients who underwent NACT and had pre- and post-treatment magnetic resonance imaging (MRI) scans. The breast parenchyma and tumors were automatically segmented using nnU-Net. Quantitative BPE metrics were calculated using multiple threshold values based on signal intensity and the signal enhancement ratio. Clinicopathological variables analyzed included age, menopausal status, body mass index (BMI), hormone receptor (HR) status (estrogen receptor, progesterone receptor), human epidermal growth factor receptor 2 (HER2) status, Ki-67 proliferation index, histologic grade, tumor and breast parenchymal volumes, and pre-/post-treatment pathological findings. The BPE parameters and clinicopathological data were evaluated using univariate and multivariable logistic regression models. Pre-specified subgroup analyses were performed using Mann–Whitney U tests, and the independence of subgroup BPE signals from menopausal status and BMI was tested in adjusted logistic models.

RESULTS

None of the evaluated quantitative BPE metrics showed a statistically significant association with pCR in the overall cohort ($P > 0.05$ for all). In pre-specified exploratory subgroup analyses, however, baseline BPE was significantly lower among patients with pCR in the HER2-negative subgroup (median 49.8% vs. 59.3%, $P = 0.014$) and in HR-positive disease (median 44.6% vs. 58.3%, $P = 0.003$), and a relative increase in BPE during NACT was associated with pCR in HR-positive tumors ($P = 0.017$). In triple-negative disease, lower post-treatment BPE accompanied pCR ($P = 0.010$). Multivariable analysis revealed that a high Ki-67 proliferation index [adjusted odds ratio (OR) 1.03 per unit, 95% confidence interval (CI), 1.01–1.04; $P = 0.0029$] and HER2 positivity (adjusted OR: 2.99, 95% CI, 1.19–7.56; $P = 0.020$) were strong and independent predictors of pCR. The diagnostic performance [area under the curve (AUC)] of the multivariable model was 0.76 (95% CI: 0.69–0.83).

CONCLUSION

Even when standardized and reproducible quantitative measurements are obtained via deep learning algorithms, BPE dynamics did not independently predict pCR in this single-center cohort; however, hypothesis-generating subgroup-specific signals in HER2-negative and HR-positive disease warrant prospective evaluation. Traditional clinicopathological features reflecting the tumor's intrinsic biology remain the most reliable determinants in this cohort for predicting NACT response.

CLINICAL SIGNIFICANCE

Although custom-trained deep learning models enable standardized and reproducible quantification of BPE, our findings show that BPE dynamics do not independently predict pCR across an unselected NACT cohort. Even a model combining BPE with clinicopathological variables achieved only modest cross-validated discrimination (AUC ≈ 0.69), and this discrimination was fully accounted for

You may cite this article as: Öncü S, Yüce M, Temur Aİ. Comparing clinicopathological factors and quantitative background parenchymal enhancement to predict pathological complete response after neoadjuvant chemotherapy in breast cancer. *Diagn Interv Radiol*. 14 September 2026 DOI: 10.4274/dir.2026.264036 [Epub Ahead of Print].

by Ki-67 and HER2 status; quantitative BPE added no incremental value. These results do not support the standalone clinical use of quantitative BPE for early response prediction. Clinicians should continue to prioritize intrinsic tumor markers (Ki-67 index, HER2 status), but the subgroup-specific BPE signals observed here are exploratory and require prospective validation before any clinical application.

KEYWORDS
Breast cancer, pathological complete response, neoadjuvant chemotherapy, background parenchymal enhancement, deep learning, nnU-Net

Neoadjuvant chemotherapy (NACT) is increasingly utilized in breast cancer management to reduce tumor size, facilitate breast-conserving surgery, and assess *in vivo* systemic therapy response.[1] A primary goal is achieving pathological complete response (pCR), defined as the total eradication of invasive cancer cells in the breast and axillary lymph nodes. Achieving pCR is a robust prognostic indicator that significantly improves overall and disease-free survival, particularly in aggressive subtypes such as triple-negative breast cancer (TNBC) and human epidermal growth factor receptor 2 (HER2)-positive breast cancer.[2]

Radiological evaluations are essential for post-treatment surgical planning and pCR prediction. Breast magnetic resonance imaging (MRI) remains the most accurate imaging modality for detecting residual disease by assessing changes in tumor vascularity, perfusion, and microstructural composition following NACT.[1] Although highly sensitive and specific, its accuracy in predicting pCR varies across different biological tumor subtypes.[3]

The characteristics of normal breast tissue distinct from the tumor are currently garnering considerable attention. Background parenchymal enhancement (BPE)—the enhancement of normal fibroglandular tissue (FGT) on dynamic contrast-enhanced (DCE) MRI—is a crucial clinical and biological biomarker.[4] Highly influenced by estrogen (ER) levels, as well as the menstrual cycle phase and menopausal status,[5] it reflects the basal metabolic activity and perfusion of normal tissue. Notably, moderate or marked BPE is significantly associated with an increased risk of developing breast cancer.[6]

Main points

- A custom-trained three-dimensional no-new-Net deep learning model enables reproducible and observer-independent quantification of background parenchymal enhancement (BPE).
- Despite rigorous objective volumetric assessment, neither baseline BPE nor its dynamic changes independently predict pathological complete response to neoadjuvant chemotherapy in the overall cohort.
- Intrinsic biological tumor markers, specifically Ki-67 proliferation index values and human epidermal growth factor receptor 2 (HER2) status, remain the most reliable independent predictors of treatment response.
- Pre-specified subgroup analyses suggest that lower baseline BPE in hormone receptor-positive/HER2-negative disease and lower post-treatment BPE in triple-negative disease may carry a response signal that is masked in the unstratified cohort.

In clinical practice, BPE is evaluated qualitatively using the American College of Radiology Breast Imaging Reporting and Data System lexicon (minimal, mild, moderate, or marked). However, this subjective assessment causes substantial inter-reader variability.[7] To eliminate this and obtain reproducible data, quantitative methods using computer algorithms have been developed to segment FGT and calculate BPE.[6,8,9] These measurements overcome visual assessment limitations by objectively determining FGT volume and BPE intensity.

A continuous decrease (suppression) in BPE is generally observed throughout the NACT process. This is thought to stem from chemotherapy-induced ovarian suppression and decreased vascularity in normal breast tissue. The absence of BPE suppression during NACT has been proposed as an early indicator of inadequate tumor response;[10,11] thus, monitoring quantitative BPE changes during chemotherapy provides a potential opportunity for early evaluation of treatment efficacy.

The relationship between BPE levels—particularly in the contralateral (healthy) breast—and pCR following NACT has become a prominent research focus.[11,12] This stromal activity, which represents high microvascular density, reflects the delivery capacity of chemotherapeutic agents to the tumor. Consequently, an early-stage decline in BPE could serve as a potential predictor of successful pCR.[13]

Accordingly, quantitatively analyzing BPE changes on pre- and post-NACT breast MRIs is crucial for elucidating their association with pCR. Beyond confirming or refuting prior reports, the present study advances the literature by (i) deploying a fully automated, dedicated three-dimensional (3D) deep learning (nnU-Net) segmentation framework that was trained and internally validated on manually corrected expert annotations and shown to be on par with inter-reader agreement; (ii) evaluating, in the same cohort, BPE quantified across two enhancement definitions [signal intensity (SI) and signal enhancement ratio (SER)] and three thresholds (> 10%, > 20%, > 30%)—an analysis space not previously reported together; and (iii) performing pre-specified subgroup analyses by molecular subtype, HER2/hormone receptor (HR) status, and menopausal status to test whether the previously reported associations between BPE and pCR are reproduced when BPE is measured in a fully objective way.[5,7]

Methods

Study population

University of Health Sciences Türkiye, Bakırköy Dr. Sadi Konuk Training and Research Hospital Ethics Committee approved this retrospective study (decision number: 2025-05-03, date: March 5, 2025), waiving the need for informed consent. Initially, 186 women with breast cancer who received NACT between January 2016 and September 2024 were evaluated. The inclusion criteria were as follows: (i) biopsy-proven unilateral invasive breast cancer; (ii) receipt of NACT; and (iii) the availability of pre- and post-NACT breast MRIs at the study institution. Among the 168 eligible patients, exclusions included the lack of post-NACT surgery at the study center (n = 4, 2.4%), subsequent identification of contralateral breast lesions (n = 2, 1.2%), or missing MRI data (n = 20, 12%). Ultimately, 142 patients (mean age, 48.9 ± 10.2 years; range, 25–86) with 284 MRI examinations were included.

Clinical and treatment data

Analyzed variables included age, menopausal status, body mass index (BMI), histologic grade (Bloom and Richardson method), biomarker status [ER, progesterone (PR),

HER2], Ki-67 proliferation index values, tumor/breast volumes, BPE percentage, and post-NACT surgical type. Tumors with > 10% nuclear immunoperoxidase staining were considered ER or PR positive, and HER2 status was evaluated via immunohistochemistry (3+ considered positive) or fluorescence *in situ* hybridization for 2+ equivocal cases (HER2/chromosome 17 centromere ratio > 2.0).[14,15] Co-expressing tumors (HR- and HER2-positive) were analyzed within the HER2-positive group, and NACT regimens were individualized through a multidisciplinary tumor board based on biological subtypes: anthracycline- and taxane-based therapies for Luminal A/B and triple-negative subtypes (with platinum agents added selectively for the latter), with targeted therapies (trastuzumab ± pertuzumab) added for HER2-positive cases.

pCR definition

pCR was defined, as per the institutional pathology protocol, as the absence of residual invasive carcinoma in the breast and ipsilateral axillary lymph nodes on the surgical specimen (ypT0/Tis ypN0) based on standardized whole-specimen sampling by a dedicated breast pathologist; residual ductal carcinoma *in situ* (DCIS) was permitted in line with current consensus.

Imaging time windows

Pre-NACT MRI was performed within 4 weeks (median 14 days) after biopsy and before the first cycle of chemotherapy. Post-NACT MRI was performed within 4 weeks (median 18 days) before definitive surgery and at least 3 weeks after the last chemotherapy administration. Because the study cohort was retrospective, patients who were premenopausal could not be systematically scheduled in the second week of the menstrual cycle; this is acknowledged as a limitation.

Magnetic resonance imaging protocol

Pre- and post-NACT MRIs were acquired on a 3-Tesla system (Magnetom Verio; Siemens Healthcare, Erlangen, Germany) using a dedicated bilateral phased-array breast coil. The standardized protocol included axial turbo inversion recovery magnitude, multi-b-value diffusion-weighted imaging, and pre-contrast T1-weighted sequences. DCE imaging utilized a fat-suppressed 3D T1-weighted gradient-echo sequence. Following a pre-contrast baseline, an intravenous gadolinium-based contrast agent (0.2 mmol/kg) was injected at 2–3 mL/s, followed by a 20-mL saline flush, alongside four post-contrast dynamic phases. Subtraction images and time–SI curves were subsequently generated (Table 1).

Image processing and background parenchymal enhancement quantification

All segmentation work was performed on the axial first post-contrast DCE T1-weighted sequence (the same volume used for BPE quantification) in NIfTI format. A radiologist (10 years of dedicated breast imaging experience) manually contoured the bilateral fibroglandular parenchyma and the enhanced tumor region on every slice in 3D Slicer (v5.8.1), explicitly excluding the nipple–areolar complex, cysts, and major vessels. The mean manual segmentation time was approximately 15–20 minutes per examination, illustrating the operational burden that motivates the automated pipeline described below.

Image registration

Pre- and post-contrast volumes of each examination were co-registered with a rigid (6 degrees of freedom) transformation in SimpleITK (Mattes mutual information metric, regular step gradient descent optimizer, multi-resolution pyramid with three levels). Registration quality was visually inspected slice by slice by the radiologist before voxel-wise subtraction; cases in which residual misregistration produced ghosting at the parenchyma–fat interface were excluded.

Automated segmentation (nnU-Net)

A 3D full-resolution nnU-Net (v2) model was trained for three-class semantic segmentation (right parenchyma, left parenchyma, tumor) on 121 patients (242 examinations, pooled pre- and post-NACT), with 21 patients (42 examinations) retained as an internal test set. Five-fold cross-validation was performed using the framework's default U-Net encoder–decoder backbone with anisotropic convolutions, instance normalization, leaky ReLU activations, and deep supervision. Mirroring augmentation was disabled (nnUNetTrainerNoMirroring) to preserve the left/right anatomical distinction required for laterality-specific BPE outputs. The supplementary schematic illustrates the overall pipeline (pre/post DCE volume, nnU-Net inference, laterality-aware parenchyma masks, voxel-wise BPE thresholding). A second radiologist independently segmented the test set to assess inter-observer variability using the Dice similarity coefficient (DSC) and Cohen's κ. The study design is presented in Figure 1.

BPE quantification

BPE was quantified using an SI approach. For parenchymal voxels, the percentage signal increase was calculated as follows: Percent Increase = [(SI_post – SI_pre) / SI_pre] × 100. Binary BPE masks were generated using 10% to 100% thresholds (in 10% increments) to compute absolute BPE volume (mL), relative BPE percentage, and mean post-contrast SI. A secondary SER was similarly calculated using late post-contrast phases (phase 4) when available: SER = (SI_early – SI_pre) / (SI_late – SI_pre). Structured BPE metrics (pretreatment, post-treatment, and delta) were extracted for the non-tumor contralateral breast as well as bilaterally. Automated BPE quantification was also validated against

Table 1. Magnetic resonance imaging protocol parameters

Sequence	TR (ms)	TE (ms)	ETL	TI (ms)	FA (°)	Matrix	Slice Thickness (mm)	Gap (mm)	FOV (cm)	Pixel size (mm)	NEX	BW (kHz)
TIRM (axial)	5,000–7,000	50–70	15–25	170–220	150	320 × 256	3–4	0.5–1	30–36	≈1.0 × 1.2	1–2	200–260
DWI (EPI)	4,000–8,000	60–90	—	—	90	128 × 128	3–4	0–1	30–36	≈2.0 × 2.0	2–4	1500–2000
Pre-contrast T1-weighted GRE (fat-saturated, 3D)	4–6	1.5–2.5	—	—	10–15	384 × 256	1–1.5	0	30–36	≈0.8 × 0.8	1	300–450
Dynamic T1-weighted GRE (fat-saturated, 3D)	4–6	1.5–2.5	—	—	10–15	384 × 256	1–1.5	0	30–36	≈0.8 × 0.8	1	300–450

TR, repetition time; TE, echo time; ETL, echo train length; TI, inversion time; FA, flip angle; FOV, field of view; NEX, number of excitations; GRE, gradient echo; EPI, echo-planar imaging; DWI, diffusion-weighted imaging; TIRM, turbo inversion recovery.

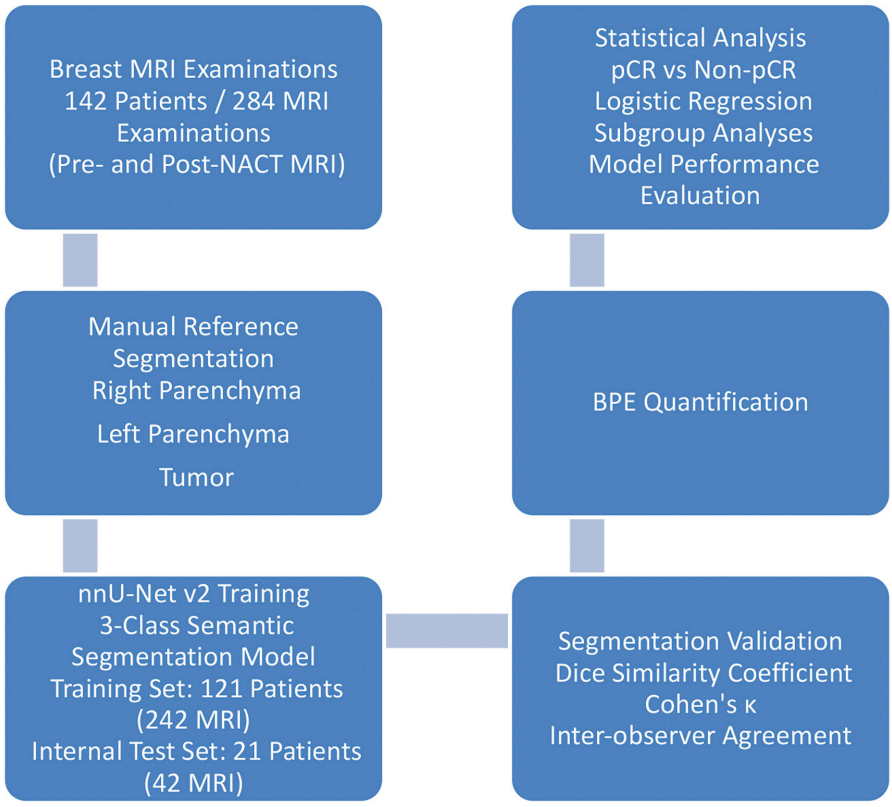

Figure 1. Flowchart of the study design. BPE, background parenchymal enhancement; MRI, magnetic resonance imaging; NACT, neoadjuvant chemotherapy; nnU-Net, no-new-Net; pCR, pathological complete response.

manual measurements using the model-generated masks.

Statistical analysis

Structured feature triplets (pretreatment, post-treatment, and delta BPE) alongside clinical variables were evaluated for predicting pCR. Univariate logistic regression was initially applied to standardized continuous variables, reporting odds ratios (ORs) per standard deviation (SD) increase. Model performance was assessed via the area under the receiver operating characteristic (ROC) curve (AUC), sensitivity, specificity, and F1 scores, with 95% confidence intervals (CIs) derived from 1,000 bootstrap iterations. Independent predictors were identified through multivariable logistic regression utilizing L1-regularized (least absolute shrinkage and selection operator) feature selection, evaluated using the apparent AUC and five-fold cross-validation. Non-parametric tests (Kruskal–Wallis, Mann–Whitney U) assessed associations between BPE and immunohistochemical subtypes. Pre-specified subgroup analyses compared BPE (pre, post, delta at the > 30% SER bilateral threshold) between patients with and without pCR in terms of the following: (i) HER2 positivity vs. HER2 negativity, (ii) HR positivity (ER+ and/or PR+) vs. HR negativity, (iii) molecular subtype strata (Luminal A/B, HER2+, TNBC), and (iv) premenopausal vs. postmenopausal status (recorded directly in the clinical database). Mann–Whitney U tests were used given the non-normal distributions in these strata; because of the exploratory nature of these subgroup analyses, nominal p-values are reported without further multiplicity correction. The associations of menopausal status and BMI with both pCR and baseline BPE were tested directly (Fisher exact, Mann–Whitney U, Spearman correlation), and a multivariable logistic model adjusting baseline BPE for age, BMI, and menopausal status was fitted within the HR-positive subgroup in which a univariate BPE signal was detected. To assess the incremental value of the full multivariable model over the two dominant clinical predictors, a parsimonious logistic model containing only HER2 status and Ki-67 was additionally fitted and compared with the full model using the same standardization, L2 estimator, five-fold cross-validation, and bootstrap procedure. The added discrimination of the remaining covariates was tested using the DeLong test on the apparent ROC curves, and the incremental contribution of the BPE terms was tested with nested likelihood-ratio tests. Analyses were conducted in Python (v3.12; scikit-learn, statsmodels, nnU-Net, 3D Slicer), with statistical significance defined as a two-sided $P < 0.05$.

Results

Cohort demographics and treatment characteristics

The final cohort comprised 142 women with a mean age of 48.9 ± 10.2 years; 77 (54.2%) were under 50 years of age and 65 (45.8%) were ≥ 50. Menopausal status was recorded directly: 69 (48.6%) were premenopausal and 73 (51.4%) postmenopausal, and the mean BMI was 28.4 ± 4.9 kg/m^2 (range 17–42). The molecular distribution was as follows: Luminal A = 5 (3.5%), Luminal B = 36 (25.4%), HER2 positive = 61 (43.0%), and triple negative = 40 (28.2%). HR positivity (ER and/or PR) was observed in 74 patients (52.1%) and HER2 positivity in 61 (43.0%). The overall pCR rate was 40.1% (57/142); pCR rates per subtype were 0% (0/5) for Luminal A, 22.2% (8/36) for Luminal B, 52.5% (32/61) for HER2 positive, and 42.5% (17/40) for triple negative [chi-square (χ^2), $P = 0.007$]. Pre-NACT axillary involvement was documented in 115/142 (81.0%) patients. The most common post-NACT surgical procedure was breast-conserving surgery with sentinel lymph-node biopsy (54/142, 38.0%).

Automated segmentation performance

In the internal test cohort, the deep learning framework demonstrated high spatial agreement with manual annotations for breast parenchyma and moderate-to-high agreement for tumor segmentation. Mean DSCs for the left and right breast parenchyma were 0.85 ± 0.10 (range 0.50–0.96) and 0.87 ± 0.13 (range 0.15–0.97), respectively. Tumor DSCs averaged 0.61 ± 0.36 (range 0.00–0.97), which improved to 0.70 ± 0.29 (range 0.00–0.97) when restricting the analysis to tumors > 100 predicted voxels. Overall tumor detection sensitivity was 0.93, with a specificity of 0.85. Applying the 100-voxel threshold maintained high sensitivity (0.90) while increasing specificity (0.92) by reducing false-positive detections.

Inter-reader and model–reader agreements were robust. For the right breast, Cohen's κ between observer 1 and the model (0.87 ± 0.13) was comparable to that of inter-observer agreement (observer 1 vs. 2: 0.86 ± 0.20) and model vs. observer 2 agreement (0.82 ± 0.19). For the left breast, the corresponding κ values were 0.85 ± 0.10,

0.88 ± 0.09, and 0.83 ± 0.12, respectively. Tumor segmentation agreement followed a similar pattern (observer 1 vs. model: 0.61 ± 0.36; observer 1 vs. 2: 0.77 ± 0.32; model vs. observer 2: 0.59 ± 0.36) (Figure 2).

Predictors of pathological complete response

Univariate analysis of clinicopathological and background parenchymal enhancement variables

Univariate analyses (Table 2) revealed that the absence of post-treatment axillary metastasis was markedly more frequent among patients with pCR (91.2% vs. 38.8%). Conversely, the presence of post-treatment axillary metastasis was associated with substantially lower odds of pCR (OR: 0.06, 95% CI: 0.02–0.17; $P = 6.88 \times 10^{-8}$; AUC: 0.76, 95% CI: 0.69–0.82). Similarly, post-treatment lymphovascular invasion ($P = 1.65 \times 10^{-9}$), DCIS ($P = 6.41 \times 10^{-7}$), and perineural invasion ($P = 0.011$) were strongly associated with lower odds of pCR. These post-treatment pathological variables are reported here as correlates of the residual disease state rather than as pretreatment predictors, and they are therefore presented separately from the candidate predictor variables in Table 2 and were not entered into the multivariable predictive model.

Among baseline tumor variables, HER2 positivity (OR: 2.47, 95% CI: 1.24–4.92; $P = 0.010$) and higher Ki-67 levels (OR 1.51, 95% CI 0.99–2.29; p = 0.0396) were associated with increased odds of pCR. Pretreatment tumor volume showed an inverse association (OR 0.63, 95% CI 0.41–0.93; $P = 0.0233$). Pretreatment axillary metastasis and ER/PR status were not significant (P > 0.05). However, the Luminal A/B subtype was significantly associated with lower odds of pCR compared to other molecular subtypes (OR: 0.26, 95% CI: 0.11–0.61; P = 0.001). Menopausal status (postmenopausal vs. premenopausal: OR: 0.76, 95% CI: 0.39–1.49; $P = 0.43$) and BMI (OR 0.82 per 1 SD, 95% CI: 0.58–1.16; $P = 0.26$) were likewise not significantly associated with pCR (Table 2). Notably, neither baseline BPE nor dynamic BPE changes demonstrated statistically significant associations with pCR in the unstratified cohort (all $P > 0.05$; AUC ≈ 0.5–0.6) (Supplementary Table 1). In addition, BPE variables showed no significant relationships with immunohistochemical molecular subtypes ($P > 0.05$) (Supplementary Table 2).

Pre-specified subgroup analyses

Within the HER2-negative subgroup (n = 81), patients with pCR had significantly lower baseline bilateral BPE than those without (median 49.8% vs. 59.3%, Mann–Whitney $P = 0.014$). Within the HR-positive subgroup (n = 74), patients with pCR had lower baseline BPE than those without (median 44.6% vs. 58.3%, $P = 0.003$) and a relative increase in BPE during NACT (median delta +6.8% vs. –3.5%, $P = 0.017$). The same direction was observed in the combined Luminal A/B subgroup (pre-BPE $P = 0.004$; delta p = 0.029, n = 41 with eight pCR events). In the triple-negative subgroup, pCR was associated with lower post-treatment BPE (median 47.7% vs. 57.9%, $P = 0.010$), whereas no BPE metric reached significance in the HER2-positive subgroup or in the pre-/postmenopausal subgroups (Supplementary Table 3). Given the small number of pCR events within each stratum, these findings should be interpreted as hypothesis-generating. Menopausal status was not associated with pCR (premenopausal 43.5% vs. postmenopausal 37.0%; Fisher exact OR 0.76, $P = 0.49$), and baseline BPE did not differ between women who were pre- and postmenopausal (median 55.3% vs. 56.8%, $P = 0.94$). Likewise, BMI was unrelated to pCR ($P = 0.23$) and showed no correlation with baseline BPE (Spearman $\rho = -0.08$, $P = 0.32$). Notably, in the HR-positive subgroup, the lower baseline BPE associated with pCR remained significant after adjustment for age, BMI, and menopausal status (adjusted OR 0.46 per 1-SD increase in BPE, $P = 0.006$), indicating that this subgroup signal is not explained by menopausal status or body habitus.

Multivariable predictive modeling

In multivariable analysis incorporating L1-regularized feature selection (Table 3, Figure 3), Ki-67 (adjusted OR 1.03 per unit increase, 95% CI: 1.01–1.04; $P = 0.0029$) and HER2 positivity (adjusted OR 2.99, 95% CI 1.19–7.56; $P = 0.020$) remained the sole independent predictors of pCR. Age, tumor/breast volumes, and BPE metrics (> 30% increase in SER) were not independently associated with pCR (all $P > 0.05$).

The multivariable model achieved an apparent AUC of 0.76 (95% CI: 0.69–0.83). At the Youden-derived threshold (0.334), sensitivity was 0.88 (95% CI: 0.64–0.98), specificity was 0.56 (95% CI: 0.46–0.81), and F1-score was 0.69 (95% CI 0.61–0.78). Five-fold cross-validation yielded an apparent AUC of 0.754 and a mean cross-validated AUC of 0.694 ± 0.075, indicating moderate generalizability.

Overall, although residual post-treatment pathological features strongly correlated with pCR, as expected from their nature as outcome-related findings, baseline proliferative activity (Ki-67) and HER2 status were the primary independent pretreatment predictors. Moreover, MRI-based BPE metrics did not independently predict pCR in the overall cohort, although exploratory subgroup analyses identified consistent BPE signals

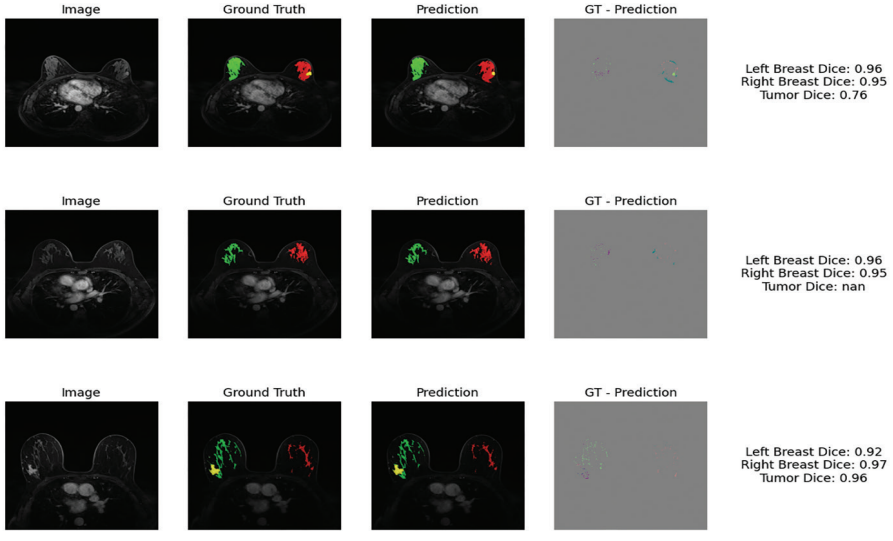

Figure 2. Deep learning-based automated segmentation of breast parenchyma and tumor. Representative axial contrast-enhanced magnetic resonance imaging slices demonstrating the performance of the nnU-Net model. Columns (left to right): original image, ground truth (GT; manual expert segmentation), automated model prediction, and the difference map (GT – Prediction). The left breast parenchyma is delineated in green, the right breast parenchyma in red, and the tumor in yellow. The corresponding Dice similarity coefficients for each class are provided on the right ("nan" tumor Dice in the middle row indicates the absence of tumor on that slice). Color legend, scale bar, and per-class Dice values are now annotated directly on the figure to improve readability.

Table 2. Univariate analysis of pretreatment clinicopathological and background parenchymal enhancement variables (primary candidate predictors). Post-treatment pathological variables are reported separately at the end of the table as descriptive outcome correlates and are not candidate pretreatment predictors

Predictor	pCR(–)	pCR(+)	OR (95% CI)	*P*	AUC (95% CI)
%Ki-67 (mean ± SD)	39.7 ± 22.1	49.0 ± 25.6	1.51 (0.99–2.29)	0.040	0.60 (0.51–0.70)
Age (years, mean ± SD)	49.1 ± 10.7	48.7 ± 9.6	0.94 (0.65–1.38)	0.763	0.52 (0.42–0.61)
Postmenopausal vs. premenopausal, n (%)	46 (54.1)	27 (47.4)	0.76 (0.39–1.49)	0.431	0.53 (0.45–0.62)
Body mass index (kg/m^2, mean ± SD)	28.8 ± 5.3	27.8 ± 4.2	0.82 (0.58–1.16)	0.264	0.56 (0.46–0.66)
HER2 positive, n (%)	29 (34.1)	32 (56.1)	2.47 (1.24–4.92)	0.010	0.61 (0.53–0.69)
ER positive, n (%)	48 (56.5)	25 (43.9)	0.60 (0.31–1.18)	0.171	0.56 (0.48–0.64)
PR positive, n (%)	35 (41.2)	20 (35.1)	0.77 (0.39–1.55)	0.488	0.53 (0.45–0.61)
Luminal A/B vs. other IHC	33 (38.8)	8 (14.0)	0.26 (0.11–0.61)	0.001	0.65 (0.57–0.73)
Invasive ductal carcinoma vs. other	72 (84.7)	56 (98.2)	10.11 (1.28–79.6)	0.008	0.57 (0.53–0.61)
Tumor grade 3 vs. 2	37 (43.5)	25 (43.9)	1.01 (0.51–1.99)	0.969	0.50 (0.42–0.58)
Pretreatment LVI present, n (%)	13 (15.3)	6 (10.5)	0.65 (0.23–1.82)	0.462	0.52 (0.47–0.58)
Pretreatment DCIS present, n (%)	9 (10.6)	6 (10.5)	0.99 (0.33–2.96)	1.000	0.50 (0.45–0.55)
Pretreatment PNI present, n (%)	1 (1.2)	2 (3.5)	3.05 CI: 0.27–34.50	0.564	0.51 (0.49–0.54)
Pretreatment axillary metastasis, n (%)	72 (84.7)	43 (75.4)	0.55 (0.24–1.29)	0.194	0.55 (0.47–0.61)
Pretreatment tumor volume (mL)	33,106 ± 64,131	17,201 ± 19,197	0.63 (0.41–0.93)	0.023	0.61 (0.51–0.70)
Pretreatment bilateral parenchymal volume (mL)	238,798 ± 201,087	220,560 ± 119,641	1.08 (0.76–1.61)	0.690	0.48 (0.39–0.58)
Pretreatment BPE% (> 30% SER, bilateral)	56.98 ± 13.06	52.88 ± 16.29	0.72 (0.47–1.09)	0.106	0.58 (0.48–0.68)
Post-treatment BPE% (> 30% SER, bilateral)	53.98 ± 10.10	52.62 ± 12.82	0.84 (0.54–1.24)	0.373	0.54 (0.45–0.64)
ΔBPE% (> 30% SER, bilateral)	−3.00 ± 14.96	−0.26 ± 16.89	1.22 (0.84–1.87)	0.324	0.55 (0.45–0.65)
Post-treatment axillary metastasis present (outcome correlate)	52 (61.2)	5 (8.8)	0.06 (0.02–0.17)	< 0.001	0.76 (0.69–0.82)
Post-treatment LVI present (outcome correlate)	34 (40.0)	0 (0.0)	0.47 (0.39–0.58)	< 0.001	0.70 (0.65–0.75)
Post-treatment DCIS present (outcome correlate)	43 (50.6)	6 (10.5)	0.11 (0.04–0.29)	< 0.001	0.70 (0.63–0.76)
Post-treatment PNI present (outcome correlate)	9 (10.6)	0 (0.0)	0.57 (0.49–0.66)	0.011	0.55 (0.52–0.59)

Continuous variables are reported as mean ± standard deviation (SD). Odds ratios for continuous variables are per 1 SD. The full structured background parenchymal enhancement table at every threshold (10%, 20%, 30% × SI/SER × bilateral/non-tumor side × pre/post/delta) is provided in Supplementary Table 1. AUC, area under the curve; BPE, background parenchymal enhancement; CI, confidence interval; DCIS, ductal carcinoma in situ; ER, estrogen receptor; HER2, human epidermal growth factor receptor 2; IHC, immunohistochemistry; LVI, lymphovascular invasion; OR, odds ratio; pCR, pathological complete response; PNI, perineural invasion; PR, progesterone receptor; SD, standard deviation; SER, signal enhancement ratio; SI, signal intensity.

Table 3. Multivariable logistic regression for pathological complete response (with adjusted odds ratios and 95% confidence intervals)

Covariate	Adjusted OR	95% CI	*P*
HER2 positive	2.99	1.19–7.56	0.020
Luminal B (vs. others)	1.62	0.64–4.12	0.312
%Ki-67 (per unit)	1.03	1.01–1.04	0.003
Pretreatment LVI present	1.71	0.45–6.49	0.430
Pretreatment BPE% (> 30% SER, bilateral)	0.69	0.44–1.08	0.104
Age	0.84	0.55–1.28	0.405
Post-treatment BPE% (> 30% SER, bilateral)	1.16	0.71–1.89	0.569
Pretreatment tumor volume (mL)	0.65	0.39–1.10	0.108
Post-treatment bilateral parenchymal volume (mL)	1.10	0.75–1.62	0.613
Pretreatment bilateral parenchymal volume (mL)	0.95	0.64–1.42	0.813

Apparent area under the curve (AUC) 0.76 [95% confidence interval (CI) 0.69–0.83]. At the Youden-derived threshold (0.334): sensitivity 0.88 (0.64–0.98), specificity 0.56 (0.46–0.81), and F1-score 0.69 (0.61–0.78). Five-fold cross-validated AUC 0.694 ± 0.075. Continuous covariates were standardized prior to regression, and their adjusted odds ratios (ORs) are expressed per 1-standard deviation (SD) increment, with the exception of Ki-67, which is reported per 1-unit (1%) increase to preserve clinical interpretability and consistency with the univariate analysis (the corresponding per-1-SD adjusted OR for Ki-67 is 1.81, 95% CI 1.23–2.66). Adjusted ORs and CIs are derived from the statsmodels logistic fit on the least absolute shrinkage and selection operator-selected feature set. LVI, lymphovascular invasion; BPE, background parenchymal enhancement; SER, signal enhancement ratio.

in HR-positive and HER2-negative disease, which merit prospective evaluation.

Incremental value of a simple HER2 + Ki-67 model

To determine how much of the model's discrimination is attributable to the two dominant clinical predictors, the full multivariable model was compared with a parsimonious model containing only HER2 status and Ki-67 (Supplementary Table 4). The HER2 + Ki-67 model alone achieved an apparent AUC of 0.71 (95% CI: 0.62–0.79) and a five-fold cross-validated AUC of 0.71 ± 0.08, with both HER2 (adjusted OR: 3.58, 95% CI: 1.66–7.74; $P = 0.001$) and Ki-67 (OR 1.81 per 1-SD, 95% CI: 1.23–2.66; $P = 0.003$) remaining significant. This is statistically indistinguishable from the full 10-covariate model (apparent AUC 0.76, cross-validated AUC 0.69–0.70): the +0.05 apparent AUC advantage of the full model was not significant (DeLong $P = 0.12$) and did not persist in cross-validation.

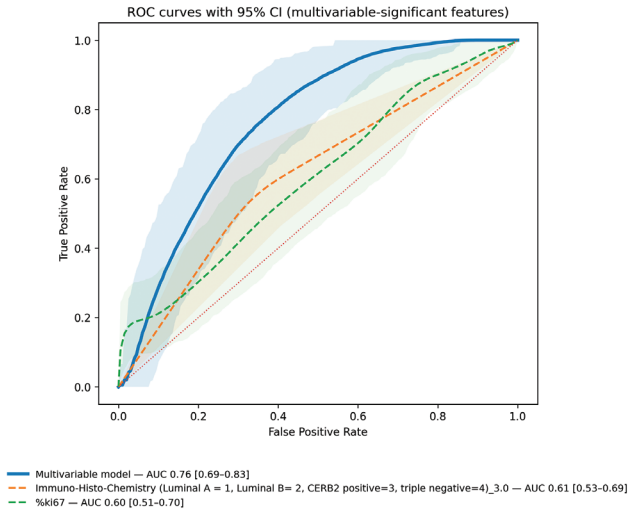

Figure 3. Receiver operating characteristic curves for predicting pathological complete response. The multivariable model [area under the curve (AUC): 0.76] outperforms immunohistochemistry subtype (AUC: 0.61) and Ki-67 proliferation index alone (AUC: 0.60). CI, confidence interval.

Adding the three BPE metrics (> 30% SER bilateral pre-, post-, and delta) to the HER2 + Ki-67 model did not improve the model fit (likelihood-ratio $\chi^2(2) = 2.58$, $P = 0.28$), and adding BPE to the full clinicopathological model was likewise non-significant ($\chi^2(2) = 3.40$, $P = 0.18$). Thus, HER2 and Ki-67 account for essentially all of the model's cross-validated discriminative performance, and neither BPE nor the volumetric covariates contribute measurable incremental value.

Discussion

In this study, we investigated the ability of nnU-Net-based quantitative BPE dynamics and clinicopathological factors to predict pCR in patients receiving NACT. Our analyses revealed that none of the BPE metrics (baseline, post-NACT, and delta BPE) demonstrated a statistically significant association with pCR in the overall cohort ($P > 0.05$). Conversely, Ki-67 proliferation index values ($P = 0.0029$) and HER2 positivity ($P = 0.020$) emerged as strong and independent predictors. Taken together with the subgroup-specific signals described below, these findings indicate—at least within an unselected single-center cohort of this size—that quantitative BPE does not provide independent predictive information beyond established clinicopathological markers, leaving open the possibility that a stratified, subtype-specific framework may extract a meaningful BPE signal.

To overcome the subjectivity and lack of standardization inherent in qualitative visual BPE assessments, a fully automated nnU-Net-based deep learning architecture was used that demonstrated concordance comparable to inter-observer agreement with expert manual segmentations (DSC: 0.85–0.87) and Cohen's κ values that matched inter-observer agreement (κ 0.82–0.88 for parenchyma). Even with this objective volumetric methodology, BPE and its dynamic changes did not independently predict pCR in the overall cohort; this is consistent with several quantitative and qualitative analyses reporting that neither baseline BPE nor its longitudinal changes are independently associated with pCR or residual disease.[13,16,17] Multivariable models integrating clinicopathological and radiological factors have likewise concluded that BPE does not emerge as an independent predictor of pCR,[18,19] corroborating our finding that only Ki-67 and HER2 status retained predictive significance in the multivariable model. Consistent with this, a parsimonious model built on HER2 and Ki-67 alone reproduced the full model's cross-validated discrimination (AUC ≈ 0.71 vs. 0.69–0.70), and adding quantitative BPE provided no incremental value (likelihood-ratio $P = 0.28$), emphasizing that the predictive signal in this cohort resides in tumor biology rather than in BPE.

The fundamental reason behind this lack of independent predictive value in unstratified cohorts is that BPE is not merely a static marker of chemosensitivity; rather, it is a highly dynamic parameter influenced by age, menopausal status, menstrual cycle phase,[5] and ER levels. Therefore, BPE suppression during NACT likely reflects a physiological reaction triggered by chemotherapy-induced ovarian suppression rather than direct tumor eradication. This physiological ambiguity is supported by large-cohort studies and systematic reviews. Analyses of the I-SPY 2 dataset, as well as comprehensive reviews, have reported that BPE reduction provides limited clinically useful prediction for pCR across unstratified cohorts, highlighting that the exact biological mechanisms altering BPE remain uncertain.[10,11,20-22] Additionally, incorporating BPE into multivariate functional tumor volume models does not substantially improve discriminatory power.[23,24]

Notably, our pre-specified subgroup analyses generated a more nuanced picture. In HR-positive and HER2-negative disease, baseline BPE was significantly lower in patients who later achieved pCR, and a relative increase rather than the expected suppression of BPE during NACT was associated with pCR. In triple-negative disease, lower post-treatment BPE accompanied pCR, whereas no BPE signal was found in HER2-positive tumors, in which the high overall pCR rate (52.5%) is dominated by HER2-targeted therapy. These subgroup-specific directions are consistent with prior reports from the I-SPY 2 and other trials, which have identified BPE–pCR associations primarily within HER2-negative or HR-positive strata,[11,24,25] providing a plausible biological reason for the negative overall result: the molecular subtypes most influenced by chemotherapy-induced ovarian suppression of BPE are also the subtypes in which baseline BPE may track underlying chemosensitivity. We refrain from drawing firm inferential conclusions from these subgroup analyses given the limited number of pCR events per stratum, but we believe they represent the most promising direction for prospective validation.

To contextualize these findings, it is crucial to examine recent studies utilizing comparable deep learning-based automated segmentation methodologies. For instance, Huang et al.[26] developed an nnU-Net model for automated BPE quantification and reported that although baseline BPE was not predictive, an early reduction in BPE (ΔBPE_{0-1}) was significantly associated with pCR. The divergence between their positive findings and our negative overall results may stem from the imaging time points evaluated; their success relied on early interim (mid-treatment) scans, whereas our analysis assessed the overall change from baseline to post-NACT. This suggests that the predictive signal of BPE might be confined to a narrow, early dynamic window. Similarly, Zhu et al.[27] employed a 3D U-Net/nnU-Net framework to automate BPE calculation, achieving optimal pCR prediction by fine-tuning and restricting the signal enhancement threshold (e.g., to

55%). By contrast, our study rigorously evaluated a comprehensive range of thresholds (10% to 100% for both SI and SER) and found no statistically significant independent association with pCR in the overall cohort across these cut-offs. This highlights that BPE's predictive value may be highly sensitive to the specific algorithmic thresholds chosen rather than acting as a robust, universal biomarker. Beyond these specific deep learning approaches, we acknowledge that a broader body of contradictory studies argues for BPE's reliability utilizing various other methodologies, such as radiomics, pharmacokinetic parameters, or qualitative visual assessments.[12,25,28-34]

However, the lack of a significant relationship in our rigorously standardized study highlights a critical vulnerability in the literature: BPE is an inherently unstable parameter highly sensitive to methodological variations. The discrepancies between our negative findings and the positive literature reports primarily stem from differences in imaging timing (early interim vs. post-NACT), measurement techniques (high-sensitivity pharmacokinetic parameters vs. standard SI), and assessment scopes (spatial radiomic heterogeneity vs. global volumetric changes). This instability is best exemplified by the conflicting results emerging from the same I-SPY 2 data pool, where different researchers found significance only by tailoring their analyses to highly specific time points, subgroup filters (HR+/HER2– vs. HR–/HER2+ to compensate for limited statistical power), or arbitrary algorithmic thresholds (e.g., optimizing high signal cut-offs over standardized ranges).[11,20,24,25] Such variability suggests that BPE change is a metric easily skewed by external factors and measurement techniques rather than a universally reliable predictor.

Our study has important limitations. It is a single-center and retrospective study, and the modest cohort size (n = 142, with 57 pCR events) constrains the statistical power of stratified analyses, particularly within the Luminal A and HER2-positive strata. Although the cohort is heterogeneous with respect to tumor subtype and individualized NACT regimens (anthracycline/taxane ± platinum for TNBC; anthracycline/taxane + trastuzumab ± pertuzumab for HER2-positive disease), this reflects routine clinical practice in our center; however, we cannot exclude that some of the observed BPE differences are mediated by regimen-specific anti-vascular and ovarian-suppressive effects rather than by tumor biology per se. Furthermore, the inability to strictly standardize premenopausal MRI acquisitions to the ideal second week of the menstrual cycle may have introduced physiological BPE fluctuations.[5] Menopausal status and BMI were recorded for the entire cohort and directly analyzed; neither was associated with pCR or with baseline BPE, and the HR-positive baseline-BPE signal persisted after adjustment for age, BMI, and menopausal status, indicating that these factors are not the principal confounders. The menstrual cycle phase at the time of imaging was nonetheless not captured in our retrospective database and remains a residual source of physiological BPE variability. Moving forward, accurate pCR prediction will likely require integrating multiparametric MRI or radiomic features reflecting the tumor's microscopic structure into multi-feature models and prospective, subtype-stratified evaluation of quantitative BPE before firm conclusions about its independent value can be drawn. A further limitation is that although the pipeline produced tumor-specific masks, these were used in this study only for tumor volume quantification and to exclude tumor voxels from the BPE measurement; we did not exploit them for intratumoral radiomic, texture, or pharmacokinetic analysis. Integrating tumor mask-derived features with parenchymal measurements in a combined model is a clear direction for future research and may recover predictive information that global volumetric and BPE metrics do not capture.

Throughout the NACT process, a quantitative reduction in breast BPE occurs due to the systemic and anti-angiogenic effects of the administered agents. However, even when measured using standardized, observer-independent deep learning models, this reduction did not function as an independent biomarker for pCR prediction in our overall cohort, although our subgroup analyses suggest that meaningful BPE–pCR signals may exist within HR-positive and triple-negative disease, meriting prospective, subtype-stratified evaluation. Clinicopathological features reflecting the intrinsic biology of the tumor itself, such as the Ki-67 index and HER2 status, remain the strongest independent determinants of NACT response in this cohort.

Footnotes

Conflict of interest disclosure

The authors declared no conflicts of interest.

Supplementary Table Link: https://d2v96fxpocvxx.cloudfront.net/beb8919b-f013-4ea1-b1c8-40332e840fe1/content-images/ace7ae45-62ca-4359-a18f-a871ace1cad2.pdf

References

1. Janssen LM, den Dekker BM, Gilhuijs KGA, van Diest PJ, van der Wall E, Elias SG. MRI to assess response after neoadjuvant chemotherapy in breast cancer subtypes: a systematic review and meta-analysis. *NPJ Breast Cancer*. 2022;8(1):107. [Crossref]
2. Antonini M, Mattar A, Pereira TM, et al. Pathologic complete response and breast cancer survival post-neoadjuvant chemotherapy: A systematic review and meta-analysis of real-world data. *Heliyon*. 2025;11(10):e43069. [Crossref]
3. Jafferbhoy S, Gowda SM, Kabeer KK, et al. Role of MRI in predicting response to neo-adjuvant systemic therapy (NAST) in breast cancer. *Breast Dis*. 2022;41:165-173. [Crossref]
4. Hu N, Zhao J, Li Y, et al. Breast cancer and background parenchymal enhancement at breast magnetic resonance imaging: a meta-analysis. *BMC Med Imaging*. 2021;21(1):32. [Crossref]
5. Kang SS, Ko EY, Han BK, Shin JH, Hahn SY, Ko ES. Background parenchymal enhancement on breast MRI: influence of menstrual cycle and breast composition. *J Magn Reson Imaging*. 2014;39(3):526-534. [Crossref]
6. Watt GP, Thakran S, Sung JS, et al. Association of breast cancer odds with background parenchymal enhancement quantified using a fully automated method at MRI: the IMAGINE study. *Radiology*. 2023;308(3):e230367. [Crossref]
7. Sogani J, Morris EA, Kaplan JB, et al. Comparison of background parenchymal enhancement at contrast-enhanced spectral mammography and breast MR imaging. *Radiology*. 2017;282(1):63-73. [Crossref]
8. Arefan D, Zuley ML, Berg WA, Yang L, Sumkin JH, Wu S. Assessment of background parenchymal enhancement at dynamic contrast-enhanced MRI in predicting breast cancer recurrence risk. *Radiology*. 2024;310:e230269. [Crossref]
9. Wei D, Jahani N, Cohen E, et al. Fully automatic quantification of fibroglandular tissue and background parenchymal enhancement with accurate implementation for axial and sagittal breast MRI protocols. *Med Phys*. 2021;48(1):238-252. [Crossref]
10. Li X, Yan F. Predictive value of background parenchymal enhancement on breast magnetic resonance imaging for pathological tumor response to neoadjuvant chemotherapy in breast cancers: a systematic review. *Cancer Imaging*. 2024;24(1):35. [Crossref]
11. Onishi N, Li W, Newitt DC, et al. Breast MRI during neoadjuvant chemotherapy: lack of

background parenchymal enhancement suppression and inferior treatment response. *Radiology*. 2021;301(2):295-308. [Crossref]

12. You C, Peng W, Zhi W, et al. Association between background parenchymal enhancement and pathologic complete remission throughout the neoadjuvant chemotherapy in breast cancer patients. *Transl Oncol*. 2017;10(5):786-792. [Crossref]
13. Rella R, Bufi E, Belli P, et al. Association between background parenchymal enhancement and tumor response in patients with breast cancer receiving neoadjuvant chemotherapy. *Diagn Interv Imaging*. 2020;101(10):649-655. [Crossref]
14. Burstein HJ, Curigliano G, Loibl S, et al. Estimating the benefits of therapy for early-stage breast cancer: the St. Gallen International Consensus Guidelines for the primary therapy of early breast cancer 2019. *Ann Oncol*. 2019;30(10):1541-1557. [Crossref]
15. Wolff AC, Hammond MEH, Allison KH, et al. Human epidermal growth factor receptor 2 testing in breast cancer: American Society of Clinical Oncology/College of American Pathologists Clinical Practice Guideline focused update. *J Clin Oncol*. 2018;36:2105-2122. [Crossref]
16. Moliere S, Oddou I, Noblet V, Veillon F, Mathelin C. Quantitative background parenchymal enhancement to predict recurrence after neoadjuvant chemotherapy for breast cancer. *Sci Rep*. 2019;9(1):19185. [Crossref]
17. Ren Z, Pineda FD, Howard FM, et al. Differences between ipsilateral and contralateral early parenchymal enhancement kinetics predict response of breast cancer to neoadjuvant therapy. *Acad Radiol*. 2022;29(10):1469-1479. [Crossref]
18. Chen P, Wang C, Lu R, et al. Multivariable models based on baseline imaging features and clinicopathological characteristics to predict breast pathologic response after neoadjuvant chemotherapy in patients with breast cancer. *Breast Care (Basel)*. 2022;17(3):306-315. [Crossref]
19. Malhaire C, Selhane F, Saint-Martin MJ, et al. Exploring the added value of pretherapeutic MR descriptors in predicting breast cancer pathologic complete response to neoadjuvant chemotherapy. *Eur Radiol*. 2023;33:8142-8154. [Crossref]
20. Nguyen AA, Arasu VA, Strand F, et al. Comparison of segmentation methods in assessing background parenchymal enhancement as a biomarker for response to neoadjuvant therapy. *Tomography*. 2020;6(2):101-110. [Crossref]
21. Philpotts LE. MRI background parenchymal enhancement and neoadjuvant chemotherapy response. *Radiology*. 2021;301(2):309-310. [Crossref]
22. Weiss J, Hunt E, Zhu Y, Duong TQ, Maldjian T. Review of prognostic significance of quantitative BPE measurements. *Diagnostics (Basel)*. 2026;16(3):495. [Crossref]
23. Kim MY, Choi N, Park S, Seo J, Ahn SY, Shin YJ. Comparison of contralateral breast background parenchymal enhancement on MRI before and after neoadjuvant chemotherapy according to molecular subtypes in unilateral breast cancer. *Diagnostics (Basel)*. 2025;15(22):2826. [Crossref]
24. Arasu VA, Kim P, Li W, et al. Predictive value of breast MRI background parenchymal enhancement for neoadjuvant treatment response among HER2 - patients. *J Breast Imaging*. 2020;2(4):352-360. [Crossref]
25. Li W, Newitt DC, Gibbs J, et al. Predicting breast cancer response to neoadjuvant treatment using multi-feature MRI: results from the I-SPY 2 TRIAL. *NPJ Breast Cancer*. 2020;6(1):63. [Crossref]
26. Huang X, Zhao Z, Dong R, et al. Automated quantification of background parenchymal enhancement in longitudinal dynamic contrast-enhanced MRI for predicting neo-adjuvant chemotherapy response in breast cancer. *Res Sq*. 2023. [Crossref]
27. Zhu Y, Hadidchi R, Nguyen HQ, et al. Automated calculation of background parenchymal enhancement as a biomarker of treatment responses and recurrence-free survival in breast cancer. *Res Sq*. 2025. [Crossref]
28. Yu Y, Wang Z, Wang Q, et al. Radiomic model based on magnetic resonance imaging for predicting pathological complete response after neoadjuvant chemotherapy in breast cancer patients. *Front Oncol*. 2024;13:1249339. [Crossref]
29. Yang W, Yang Y, Zhang C, Yin Q, Zhang N. A clinicopathological-imaging nomogram for the prediction of pathological complete response in breast cancer cases administered neoadjuvant therapy. *Magn Reson Imaging*. 2024;111:120-130. [Crossref]
30. Ren Z, Pineda FD, Howard FM, et al. Bilateral asymmetry of quantitative parenchymal kinetics at ultrafast DCE-MRI predict response to neoadjuvant chemotherapy in patients with HER2+ breast cancer. *Magn Reson Imaging*. 2023;104:9-15. [Crossref]
31. Xu L, Zhou F, Su L, Wang L. Quantitative dynamic contrast-enhanced MRI parameters effectively predict treatment efficacy of neoadjuvant chemotherapy in breast cancer. *Am J Transl Res*. 2025;17:1039-1048. [Crossref]
32. La Forgia D, Vestito A, Lasciarrea M, et al. Response predictivity to neoadjuvant therapies in breast cancer: a qualitative analysis of background parenchymal enhancement in DCE-MRI. *J Pers Med*. 2021;11(4):256. [Crossref]
33. Chalfant JS, Mortazavi S, Lee-Felker SA. Background parenchymal enhancement on breast MRI: assessment and clinical implications. *Curr Radiol Rep*. 2021;9:10. [Crossref]
34. Thomas J, Malla L, Shibwabo B. Advances in analytical approaches for background parenchymal enhancement in predicting breast tumor response to neoadjuvant chemotherapy: a systematic review. *PLoS One*. 2025;20:e0317240. [Crossref]